Report No.
UCB/SEMM-2012/03

Structural Engineering
Mechanics and Materials

Seismic Responses of 20-story Base-isolated and Fixed-base RC Structural Wall Buildings Subjected to Near-fault Ground Shaking

By

Vladimir Calugaru and Marios Panagiotou

December 2012

Department of Civil and Environmental Engineering
University of California, Berkeley

SUMMARY

This study investigates numerically the seismic response of six seismically base-isolated (BI) 20-story reinforced concrete buildings and compares their response to that of a fixed-base (FB) building with a similar structural system above ground. Located in Berkeley, California, 2 km from the Hayward fault, the buildings are designed with a core wall that provides most of the lateral force resistance above ground. For the BI buildings, the following are investigated: two isolation systems, isolation periods equal to 4, 5, and 6 s, and three levels of flexural strength of the wall. The first isolation system combines tension-resistant friction pendulum bearings and nonlinear fluid viscous dampers (NFVDs); the second combines low-friction tension-resistant linear bearings, lead-plug rubber bearings and NFVDs. The designs of all buildings satisfy ASCE 7-10 requirements, except that one component of horizontal excitation is used in the two-dimensional nonlinear response history analysis. Analysis is performed for a set of ground motions scaled to the design earthquake (DE) and to the maximum considered earthquake (MCE). At both the DE and the MCE, the FB building develops large inelastic deformations and shear forces in the wall, and floor accelerations. At the MCE, four of the BI buildings experience practically elastic response of the wall, and floor accelerations and shear forces are 0.25 to 0.55 times these experienced by the FB building. This study also investigates the response of the FB and four of the BI buildings to four historical near-fault ground motions that include strong long-period pulses.

KEY WORDS: near-fault; plastic hinge; seismic base-isolation; structural wall; tall buildings;

1. INTRODUCTION

Construction of buildings exceeding 50 m in height, referred herein as "tall" buildings, is increasing in earthquake-prone regions of the United States (U.S.) and worldwide. Common structural systems used in the seismic design of these buildings are reinforced concrete (RC) structural walls (for brevity referred to as “walls”), including also non-planar core walls [1].

Considerable damage of tall RC wall buildings in past earthquakes has been reported, including the 1985 magnitude 8 (M8.0) Mexico earthquake [2], the 2010 M8.8 Chile earthquake [3], and the 2011 M6.3 Christchurch, New Zealand, earthquake [4]. These buildings were not designed according to the provisions considered here. In the 1999 M7.6 Chi-Chi, Taiwan, earthquake [5], tall RC frame buildings—the most common type of RC tall buildings close to the fault rupture (less than 10 km)—suffered severe damage or collapsed. In the Mexico and Chile subduction-zone earthquakes severe damage and collapse of tall RC wall buildings occurred far from the fault rupture, 400 km [6] and 35 km [7], respectively, due partly to amplification of the long-period content of the ground motions at soft-soil sites.

Conventional tall RC wall buildings in the U.S. are designed to develop the majority of expected deformations in a single flexural plastic hinge, usually located near ground [1, 8-10]. Design forces are typically calculated using the code-prescribed design earthquake (DE) spectra with modal response spectrum analysis (MRSA) as prescribed

in ASCE 7-10 [11], using a response modification factor, *R*, equal to 5; RC structural members are designed according to ACI 318-11 code provisions [12]. Minimum performance objectives of ASCE 7-10 require withstanding the maximum considered earthquake (MCE) with a low probability of either partial or total collapse, and withstanding the DE that is two thirds that of the MCE, thereby ensuring life-safety. These requirements do not address post-earthquake structural or non-structural damage. In addition to code provisions, several groups have developed *ad hoc* procedures on performance, analysis, and design requirements for conventional tall buildings [13-16].

The seismic response of 20-story tall RC wall buildings designed according to Eurocode 8 has been studied numerically indicating the significant contribution of higher modes to response [17]. Numerical studies have investigated the seismic response of 40- to 42-story tall RC core wall buildings located in California subjected to DE and MCE levels of shaking for sites of high seismicity [1, 8], as well as to pulse-type near-fault ground motions [9, 10]. These studies showed that for the MCE as well as for near-fault ground shaking these buildings develop significant inelastic deformations with 2% to 3% interstory drift ratios, large shear stresses in the walls that approach the upper limit allowed by ACI 318-11, and floor accelerations that approach or even exceed peak ground acceleration (PGA). This magnitude of inelastic deformations and shear stresses can result in major post-earthquake structural and non-structural damage, requiring expensive repairs and loss of functionality. The response of 20-story tall RC core wall buildings to near-fault ground shaking has also been investigated [9, 10].

Seismic base-isolation (BI) has been used as a design strategy for tall buildings to reduce accelerations, forces, and inelastic deformations in the superstructure (structure above the isolation system) and thus earthquake-induced structural and non-structural damage. This is achieved by concentrating the majority of deformations in robust isolation systems and by reducing higher mode response.

Today a variety of seismic isolation devices that have the force and displacement capacities required to isolate tall buildings are commercially available. These devices include large (1.5 m-diameter) rubber bearings [18], large friction pendulum bearings [19], and large linear bearings [20]. Friction pendulum bearings and linear bearings with strength in tension up to 9 MN are also commercially available [19, 20]. Rubber and linear bearings have horizontal displacement capacities up to about 1 m, while that of friction pendulum bearings is up to 1.5 m. Fluid viscous dampers with a displacement capacity up to about 1.5 m are also commercially available [21]. Such devices have been experimentally tested [18-24].

Japan is the leading proponent of applying seismic isolation in tall buildings [25, 26]. Between 1990 and 2002, one-third of all the approved base-isolated (BI) buildings in Japan were taller than 40 m, and 40% of all BI buildings built in Japan after 1995 had a height-to-length ratio larger than two [25].

In the U.S., ASCE 7-10 permits the design of the structure above the isolation system of BI buildings for forces smaller than that required for elastic response at the DE; the isolation system is required to have force and displacement capacity larger than the expected demand at the MCE. Numerical studies have investigated the response of BI RC or steel frames using two-degree-of-freedom models [27] or modeling the 6 stories [28], 9 stories [29], 15 [30], 18 or 40 stories [23] of the superstructure. These studies show that the level of inelastic response of the superstructure depends on the relative characteristics of the superstructure and isolation system, as well as on ground motion characteristics. A seismic response study of the Los Angeles City Hall [31] is the only

currently available study of a tall BI building with structural walls designed to resist most of the seismic forces along a part of the building height.

This study investigates numerically the seismic response of six BI RC structural wall buildings with 20 stories above ground and compares their response to that of a fixed-base (FB) building of similar superstructure. All seven buildings are located at a site of high seismic hazard in Berkeley, California, 2 km from the Hayward fault, and are designed according to ASCE 7-10 except that one horizontal component of ground excitation is used in the two-dimensional (2-D) nonlinear response history analysis (NRHA). The NRHA is performed using a set of ground motions scaled to the DE and the MCE. The FB building and four of the BI buildings are also subjected to the unscaled fault-normal horizontal component of four historical near-fault ground motions that include strong long-period pulses.

This study addresses the following three questions: (1) Using the response of the FB building as a benchmark, is it feasible to use commercially available seismic isolation devices for the BI buildings at both the DE and the MCE to reduce significantly the level of inelastic deformations, shear forces, and floor accelerations of the superstructure; (2) What is the relation between the flexural strength of the isolated superstructure, the characteristics of the isolation system, and the level of inelastic deformations the isolated superstructure develops at the DE and MCE?; and (3) if it is possible for the four BI buildings subjected to the four unscaled near-fault ground motions to experience significantly smaller responses in the superstructure compared to the FB building without exceeding the capacity of the isolation system.

2. SITE AND GROUND MOTIONS

The buildings are hypothetically located at a site in downtown Berkeley, California, with soil type C, 2 km from the Hayward fault. The site seismic hazard and corresponding smooth design spectra are in accordance with ASCE 7-10 at both DE and MCE levels; see Figure 1. Uni-axial horizontal excitation is used in this 2-D study. Two sets (Set 1 and Set 2) of fourteen ground motions each are linearly scaled such that their mean spectrum for 5% damping ratio, ζ, approximately matches the smoothed DE and MCE design spectra over specific period ranges of interest. Sets 1 and 2 are used to analyze and compare the responses of the FB and BI buildings, respectively. The ground motion sets consist of fault-normal components of near-fault pulse-type ground motions (see Table 1). The first set approximately matches the design spectra in the period range between 0.7 s ($0.35T_1$) to 4 s ($2T_1$), where T_1 = 2 s is the first mode period of the FB building. For periods between 0.3 s and 0.7 s, the mean spectra of set 1 is 20% less on average than the design spectra. The second set matched the design spectra in the period range 1.9 s to 10.0 s, which includes the required range, per ASCE 7-10, of $0.5T_D$ to $1.25T_M$. Here, T_D = 3.7 s and T_M = 5.8 s is the effective period of the isolation system of the BI buildings (shortest T_D and longest T_M) at the design and maximum displacement, respectively. The mean scale factor at the MCE for Sets 1, and 2 of the motions is 1.43, and 1.55, respectively (see Table 1).

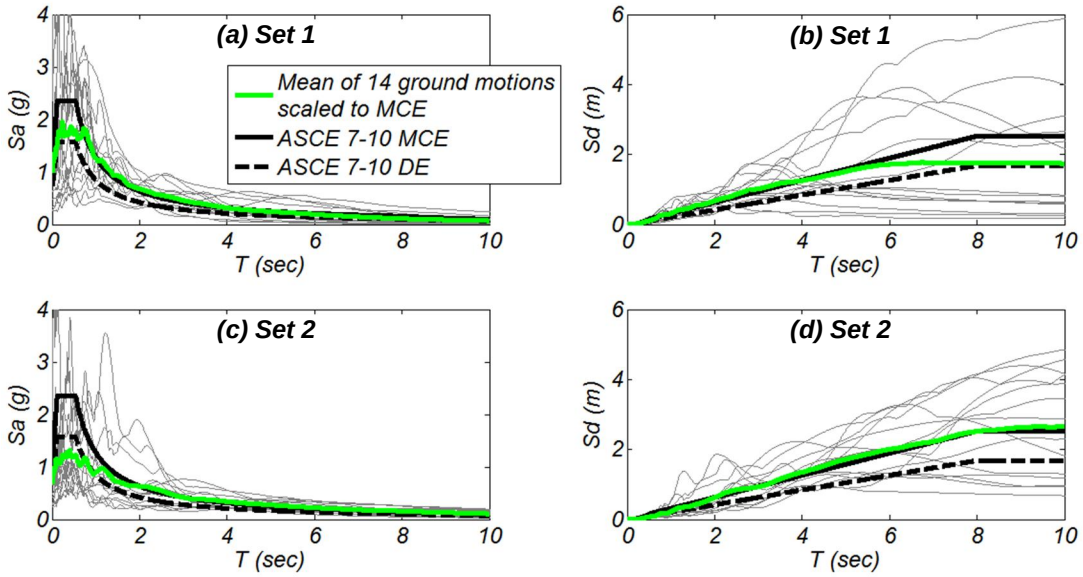

Figure 1. Linear acceleration and displacement spectra of the two sets of ground motions scaled to the MCE; DE and MCE design spectra.

Table 1. Ground motions and scale factors at the DE- and MCE-levels of shaking.

Ground motions set	Station name	Earthquake Location, Year, Magnitude	Scale factor	
			DE	MCE
Set 1 Fixed-base building	Duzce	Duzce, Turkey, 1999, M7.1	1.67	2.50
	Jensen Filter Plant	Northridge, CA, 1994, M6.7	0.43	0.65
	Rinaldi Receiving Station		0.97	1.45
	Sylmar Converter Station		0.93	1.39
	Los Gatos	Loma Prieta, CA 1989, M6.9	1.00	1.50
	Meloland Overpass	Imperial Valley, CA, 1979, M6.5	0.85	1.28
	Mianzhuqingping	Wenchuan, China, 2008, M7.9	1.66	2.50
	PRPC	Christchurch, NZ, 2011, M6.3	0.67	1.01
	Tabas	Tabas, Iran, 1978, M7.4	1.00	1.50
	Takatori	Kobe, Japan, 1995, M6.9	0.33	0.50
	TCU068	Chi-Chi, Taiwan, 1999, M7.6	0.34	0.51
	TCU084		0.36	0.54
	TCU102		1.44	2.16
	TCU129		1.67	2.50
Set 2 Base-isolated buildings	Duzce	Duzce, Turkey, 1999, M7.1	0.78	1.18
	El Centro Array #6	Imperial Valley, CA, 1979, M6.5	1.48	2.22
	Lucerne	Landers, CA, 1992, M7.3	0.31	0.47
	Mianzhuqingping	Wenchuan, China, 2008, M7.9	1.63	2.45
	Tabas	Tabas, Iran, 1978, M7.4	0.27	0.40
	Takatori	Kobe, Japan, 1995, M6.9	0.67	1.00
	TCU52	Chi-Chi, Taiwan, 1999, M7.6	0.67	1.00
	TCU67		1.67	2.50
	TCU68		0.45	0.67
	TCU87		1.06	1.59
	TCU101		1.35	2.02
	TCU102		1.52	2.29
	TCU103		1.67	2.50
	Yarimca	Kocaeli, Turkey, 1999, M7.4	0.75	1.12

3. DESCRIPTION AND DESIGN OF BUILDINGS

Figure 2 shows the main features, and Table 2 lists the main properties of the FB and BI buildings. A core wall coupled through the floor slabs with columns in the perimeter of the buildings comprises the structural system above ground. Concrete with specified compressive strength $f_c^{'}$ = 48 MPa and steel with specified yield strength f_y = 414 MPa are used. The corresponding expected material properties used in the analysis are $f_{c,e}^{'}$ = 72 MPa and $f_{y,e}$ = 455 MPa. Table 2 lists the longitudinal reinforcement ratio, ρ_l, of the wall, the axial load of the wall at the ground level, P, divided by the cross-sectional area of the wall A_g times $f_{c,e}^{'}$ as well as the flexural strength (using expected material properties) of the wall section at the ground level, M_b, for bending about the Y-axis when the outer longitudinal reinforcement of the wall reaches 1% tensile strain. The 1 m x 1 m columns have a ρ_l equal to 1.0%. The slab reinforcement consists of #5 bars every 0.3 m in the two horizontal directions, both top and bottom. Below ground a grid of RC walls is used to distribute forces to the foundation and isolation system. The layout of the isolation systems of the BI buildings is shown in Figures 2(c) and (d). For the BI buildings the seismic weight of each floor below ground is 1.5 times that of each floor above ground. A stiff diaphragm consisting of a RC slab and RC beams is assumed that is used in the isolation systems (above and below the isolation devices). Uni-axial seismic excitation along the X-axis is considered for all buildings.

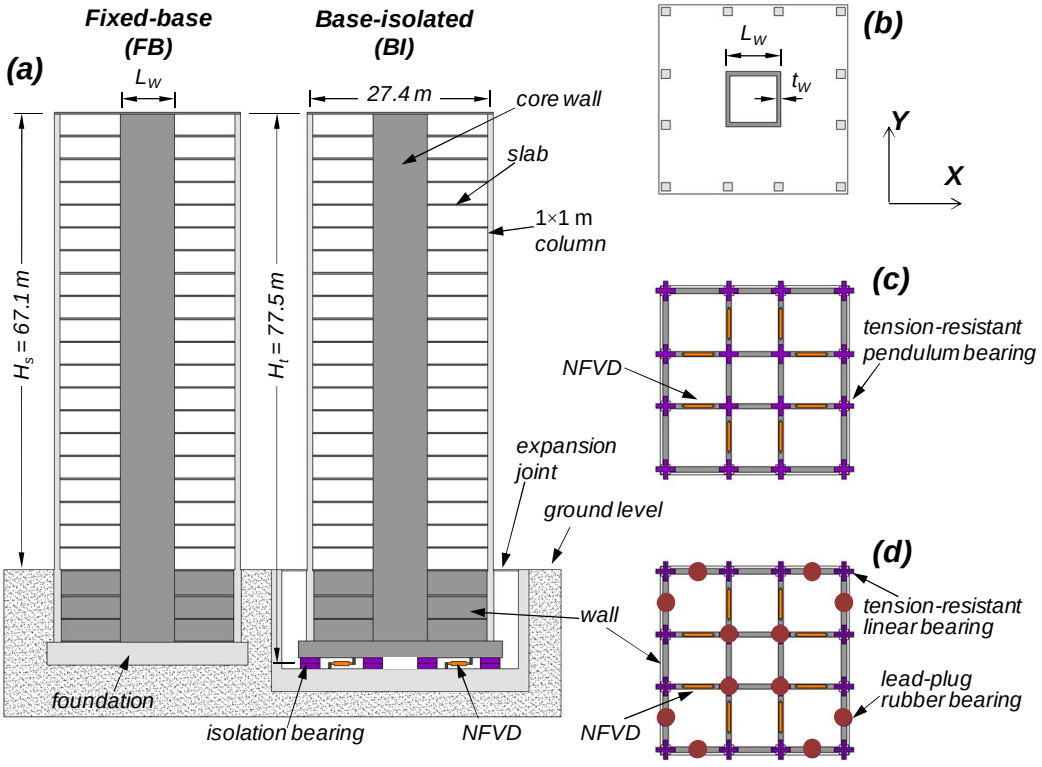

Figure 2. (a) Elevation of the 20-story buildings; (b) Floor plan-view above ground; (c) Plan-view of isolation system 1; (d) Plan-view of isolation system 2.

Table 2. Characteristics of the seven buildings.

	Building type	Fixed base	BI T_{is}=4 s	BI T_{is} = 5 s		BI T_{is} = 6 s		
	Building name	FB	BI4	BI5a	BI5b	BI6a	BI6b	BI6c
	Type of isolation system	N/A	Isolation system (IS) 1					IS2
Superstructure	Total seismic weight, W_t (MN)	154*	200	207	200	206	200	206
	Core wall length, L_w (m)	9.1	9.1	10.4	9.1	9.1	9.1	9.1
	Core wall thickness, t_w (m)	0.51	0.51	0.61	0.51	0.61	0.51	0.51
	Wall long. reinf. ratio, ρ_l (%)	1.0	1.2	2.0	1.2	2.0	1.2	2.0
	Wall axial load ratio, $100P/\left(A_g f'_{c,e}\right)$	5.3	5.3	4.5	5.3	4.8	5.3	4.8
	M_b of wall at ground level (MN-m)	644	711	1438	711	1130	711	1130
Isolation system	Curv. radius of pend. bearing R_p (m)	N/A	4.0	6.2		9.0		N/A
	Diameter of LPRBs** (m)		N/A					1.5
	Numb. of 13 mm thick rubber layers							42
	Diameter of lead-plug (mm)							254
	NFVD constant C_{ND}(MN-s$^{0.3}$/m$^{0.3}$)		N/A	0.67		0.84		1.68
	K_{is} (MN / m)		50	33.4	32.3	22.9	22.2	22.6

Notes *: For the FB building only the part above ground is considered (W_s=W_t), ** G_r=0.6 MPa, G_L=150 MPa, τ_L =10 MPa, h_L=680 mm.

3.1 Fixed-base (FB) building

For this building, the majority of inelastic deformations would typically be expected to concentrate at a single flexural plastic hinge in the wall near ground level. Modal response spectrum analysis as prescribed in ASCE 7-10 with a response modification factor of R = 5, and the square root of sum of squares (SRSS) modal combination rule is used to obtain the design lateral forces. The design base shear force is $V_u = 0.093W_t$ (W_t: the total seismic weight of the building – see Table 2). The wall is designed to resist the design moment ignoring the contribution of framing action between the wall, the slab, and the columns.

3.2 Base-isolated (BI) buildings

Six BI buildings are studied. Five of them (BI4, BI5a, BI5b, BI6a, and BI6b) use isolation system 1, described in Section 3.2.1, while building BI6c uses isolation system 2 also described in Section 3.2.1. It is assumed that both isolation systems are designed in such a way in order for the isolation devices to be replaceable. The main characteristics of the isolation devices used in the isolation systems are listed in Table 2. The horizontal static force versus horizontal static displacement of both isolation systems is idealized with the bilinear relation shown in Figure 3(a). Three isolation periods, T_{is} = 4, 5, and 6 s, are investigated where $T_{is}=2\pi\sqrt{m_t/K_{is}}$, m_t is the total mass of the building and K_{is} the post-yield tangent stiffness of the isolation system [see Figure 3(a)]. The number after "BI" in the name of each of the six BI buildings describes the T_{is} of the building (see Table 2). The design of the wall above the ground level of the six BI buildings is described in Section 3.2.2.

3.2.1 *Isolation systems*

Isolation system 1: As shown in Figure 2(c), this isolation system combines 16 tension-resistant friction pendulum bearings and 8 nonlinear fluid viscous dampers (NFVDs). Commercially available tension-resistant friction pendulum bearings consist of two orthogonal cylindrical rails interconnected by a housing slider assembly permitting sliding in two orthogonal directions [19]. These bearings have significant displacement capacity (up to 1.5 m), a tension force capacity up to 9 MN, and a compression force capacity up to 133 MN [19]. Statically, the horizontal force versus horizontal displacement relation of this isolation system when loaded with vertical force F_V is shown in Figure 3(a) with the sliding stiffness $K_{is} = |F_V| / R_P$, where R_P is the radius of curvature of the pendulum bearings (see Table 2). Note that the relation between K_{is}, R_p, and F_V is maintained both for compression and tension force F_V. A friction coefficient μ = 0.03 is used resulting in $F_y = 0.03W_t$ which is more than the required resistance to wind equal to $0.017W_t$ according to ASCE 7-10. For all the pendulum bearings Δ_y = 2 mm. The force-velocity relation of each of the NFVDs used is $F_{ND} = \text{sgn}(V)C_{ND}|V|^{\alpha}$, where F_{ND} is the damper force, C_{ND} is the damper constant (see Table 2), V the velocity, and α=0.3 is the nonlinearity factor. Building BI4 does not use NFVDs.

Isolation system 2. As shown in Figure 2(d) this isolation system combines 12 very low-friction (μ = 0.3%) tension-resistant linear bearings, 12 lead-plug rubber bearings (LPRBs), and 8 NFVDs with α = 0.3. Commercially available tension-resistant linear bearings consist of two orthogonal flat rails permitting sliding in two orthogonal directions. Linear bearings with deformation capacity up to 1 m [20] are capable of resisting large tension (up to 8.7 MN) and compression (up to 61 MN) forces, and have been used in recent large-scale shake table tests [24]. Commercially available 1.5-m-diameter LPRBS [18] have a horizontal displacement capacity of about 1 m and vertical compression force up to 40 MN. The displacement capacity of these bearings typically is determined at the point where the rubber reaches 250% shear strain or when the displacement reaches two thirds of the diameter of the bearing. The latter is a limit that depends on the level of the vertical force the bearing resists [32]. The lead-plug has a diameter equal to 254 mm and height h_L = 680 mm. The rubber layers are 13 mm thick. For this isolation system $K_{is} = 12G_rA_r/t_r$ where G_r = 0.6 MPa the shear modulus of rubber, t_r is the total thickness of rubber in each LPRB, and A_r is the cross-sectional area of the rubber in each LPRB. Also $K_0 = 12(G_LA_L/h_L + G_rA_r/t_r)$, and $\Delta_y = \tau_L h_L/G_L$ where G_L =150 MPa the effective shear modulus of lead, τ_L = 10 MPa the yield stress of lead, and A_L the cross-sectional area of the lead-plug. For all the above, $K_0 = 6.9K_{is}$. The design of this isolation system assumes a loose-bolt connection between the LPRBS and the RC slab, and beams comprising the diaphragm of the isolation system, in order not to induce tension in the LPRBs. The main difference in the horizontal force-horizontal displacement [see Figure 3(a)] of isolation systems 1 and 2 is that the latter has a smaller K_0.

3.2.2 *Isolated superstructure*

Three levels of flexural strength of the walls are studied in the six BI buildings. The design base shear force of the superstructure of all BI buildings exceeds $V_u = 0.098W_t$ as required per ASCE 7-10. Using the first mode lateral force distribution, computed with modal analysis as described in Section 5.1, to distribute V_u along the height of the

building results in a design bending moment at the ground level that ranges between $M_{u,min} = 0.37H_tV_u$ and $M_{u,min} = 0.39H_tV_u$ for the six BI buildings where H_t the building roof height from the isolation system (see Figure 2). Buildings BI4, BI5b, and BI6b use a wall (see Table 2) with M_b that is 1.1 times $M_{u,min} / \varphi$ where $\varphi = 0.9$ is the strength reduction factor for flexure; buildings BI6a and BI6c use a wall with M_b equal to 1.8 times $M_{u,min} / \varphi$; while building BI5a uses a wall with M_b equal to 2.2 times $M_{u,min} / \varphi$.

4. NUMERICAL MODELING

This 2-D numerical study uses the Open System for Earthquake Engineering Simulation (OpenSees) software [33]. The numerical model is shown in Figure 3(b). Fiber-section force-based nonlinear beam-column-elements are used to model the RC wall and columns above ground. Material models Concrete03 and Steel02 are used for concrete and steel, respectively. One element per story with four integration points is used, for the walls and the columns. All slabs are modeled using beam-with-hinges elements, with a 0.9-m-long fiber-section plastic hinge at the ends of each element. The full width of the slab is considered effective in resisting bending. Horizontal rigid linear beam elements are used to model the length of the wall at each story. Linear beam elements of high rigidity are used to model the superstructure below ground. P-delta geometric transformation is used in all beam elements. The model does not account for flexure-shear interaction, bar buckling, or bar fracture in the RC members. The FB building is modeled fixed at the ground level. Expected material properties (see Section 3) for concrete and steel are used in the analysis. The elastic modulus, and the strain-hardening factor of steel are $E_s = 200$ GPa, and $b = 0.02$, respectively.

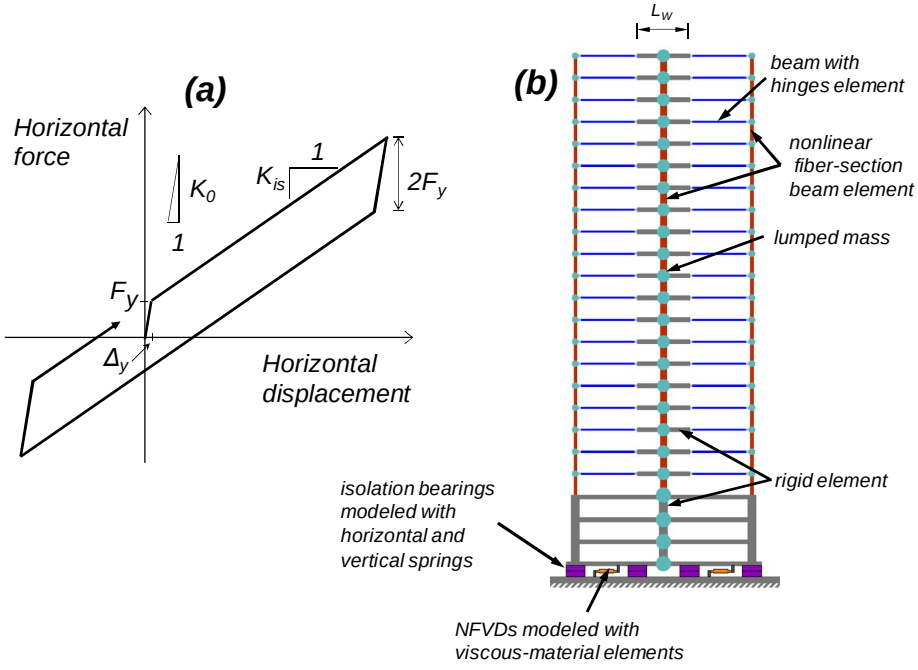

Figure 3. (a) Idealization of horizontal force (static) versus horizontal displacement of the two isolation systems; (b) Schematic of the numerical model of the BI buildings.

Vertical and horizontal zero-length spring elements are used to model the force-displacement behavior of the isolators in the corresponding direction. Modeling the

dependence between sliding stiffness, K_{is}, of the friction pendulum bearings and the vertical force acting on them was investigated and found to have a negligible effect on all the response quantities except the horizontal force of the individual pendulum bearings and the horizontal force distribution in the diaphragm of the isolation system. For this reason, this interaction is not modeled in this study. The interaction between vertical force and horizontal stiffness in the LPRBs is also ignored. A bilinear horizontal force-horizontal displacement relation is used to model the LPRBs and the tension-resistant friction pendulum bearings. The vertical stiffness in compression, and tension used for the tension-resistant pendulum bearings and the tension-resistant linear bearings is $K_{v,c}$ = 12 MN/mm and $K_{v,t}$ = 1.2 MN/mm, respectively. The NFVDs are modeled as zero length elements, with an assigned viscous material with the force-velocity relationship $F_{ND} = \text{sgn}(V)C_{ND}|V|^{\alpha}$. Rayleigh initial stiffness and mass proportional damping with 2% damping ratio in the first and the third mode is used. Horizontal and vertical lumped masses are used at three nodes per floor. Vertical forces due to gravity are applied at the same nodes.

5. RESULTS OF NUMERICAL ANALYSIS

5.1 Modal Analysis

Table 3 lists the first-mode period, T_1, and first-mode mass, m_1, divided by m_t. In all buildings cracked concrete material properties are used in the modal analysis, with the following effective flexural rigidities: (1) E_cI_e=0.25E_cI_g for the base story of the wall and the columns; (2) E_cI_e=0.5E_cI_g for the walls and the columns above the base story; and (3) 0.35E_cI_g for the slabs where I_g is the gross-section moment of inertia and E_c = 40 GPa the concrete elastic modulus. In the modal analysis the isolation systems are modeled using the stiffness K_{is} [see Figure 3(a)]. For the BI buildings the first mode mass m_1 is 0.99M_t. Thus when the isolation system responds with the tangent stiffness K_{is}, the contribution of the higher modes of response is expected to be negligible. Table 3 also reports the first mode bending moment at the ground level, $M_{1,b}$, divided by the first mode shear force at the isolation level, $V_{1,iso}$. Note that the ratio of $M_{1,b}$ / $V_{1,iso}$ ranges between 0.37H_t and 0.39H_t.

5.2 Response History Analysis using Sets of Motions Scaled to the DE and MCE

Arithmetic mean (for brevity referred to as mean) values of different response parameters of the seven buildings are summarized in Table 3 and shown in Figure 4 for the DE and MCE level of excitation. For each of the DE and MCE level of excitation, the mean values obtained from the analysis using a set consisting of 14 ground motions are reported. The responses are presented in terms of height, h_i, of floor i from the ground level, divided by the roof height above the ground level, H_s. The presented responses are the horizontal displacement relative to the base of the building (ground level for the fixed-base, base of isolation system for the BI buildings, respectively), D_i, divided by H_s, the interstory drift ratio, Θ_i, the shear force of the wall, V_i, divided by W_s (the seismic weight of the structure above ground), and the absolute floor acceleration A_i. Floor accelerations and shear forces are filtered with a finite impulse response low-

pass filter order 5000 and 20 Hz cut-off frequency, to remove numerically induced spikes due to sudden changes in the tangent modulus of the materials used.

The FB building develops significant inelastic deformations in the wall at the DE and MCE where the roof drift ratio reaches 1.22%, and 1.75%, respectively. The corresponding peak interstory drift ratios along the building height are 1.45% and 2.13%. The peak longitudinal reinforcement tensile strain in the wall (for brevity referred to as wall tensile strain) is computed at the bottom story and is 2.10% and 2.75% at the DE and MCE, respectively. At the MCE, low levels of inelastic deformations developed in the columns and the floor slabs (less than 0.37% tensile strain in the longitudinal reinforcement). For the above response parameters: the values at the MCE are 1.3 to 1.5 times the values at DE.

For the DE and MCE hazard level, the shear force in the wall at the ground level is $0.30W_s$ and $0.33W_s$, respectively, corresponding to a shear stress in the web of the wall, τ_w, of $0.068\,f_{c,e}^{'}$ and $0.075\,f_{c,e}^{'}$ approaching the maximum allowable stress of $0.078\,f_{c,e}^{'}$ ($8\sqrt{f_{c,e}^{'}}$ in psi) prescribed in ACI 318-11. Such high level of shear stresses with concurrent significant inelastic deformations in the plastic hinge region of a wall resisting large vertical force ($P=0.053f_{c,e}^{'}A_g$) can result in major damage including crushing of concrete and bar buckling. Note that the computed base shear force significantly exceeds the design base shear force. This is due to the significant contribution of higher modes in the response of tall RC wall buildings [8-10,16, 17].

Results of experimental studies have shown that non-planar walls [34, 35, 36] subjected to cyclic static loading develop major damage for drift ratios 1.5% to 2.5%. C-shape walls with ρ_l = 0.8% to 1.1%, and P = 0.059 $f_c^{'}A_g$ to 0.065 $f_c^{'}A_g$ experienced bar buckling at 2% drift ratio and vertical crushing of concrete at 2.25% to 2.5% drift ratio [34]. T-shape wall specimens with ρ_l = 1.2%, P = 0.074 $f_c^{'}A_g$ to 0.087 $f_c^{'}A_g$ [35] experienced longitudinal bar buckling at 1.5% to 2.0% drift ratio. A U-shape wall specimen with ρ_l = 1.0%, and P = 0.045 $f_c^{'}A_g$ [36] experienced web crushing at 2.5% drift ratio. The maximum shear stress of the web at crushing of this specimen was 0.06 $f_c^{'}$ ($f_c^{'}$ = 54.7 MPa), which is only 0.67 times the maximum shear stress allowed by ACI 318-11.

Considered as an average value along the height of the building, the FB building develops large floor accelerations of 0.63 g [1.2 times peak ground acceleration (PGA)] and 0.83 g (1.1 times PGA) at the DE and MCE, respectively.

Presented next is the mean response of the buildings BI5a and BI6a, which use isolation system 1 and a wall with M_b equal to 2.2 and 1.8 times, respectively, the minimum required. The superstructure of these buildings experiences elastic response at the MCE; the computed wall tensile strain is less than 0.22%. At the MCE the interstory drift ratio for these buildings is only 0.30% to 0.32% (as opposed to 2.13% for the FB). For this level of interstory drift ratio, standard gypsum partitions remain undamaged [37]. The roof drift ratio of these buildings is 0.81% to 0.82% at DE (as opposed to 1.22% for the FB) and 1.53% to 1.6% at the MCE (as opposed to 1.75% for the FB).

Buildings BI5a and BI6a develop horizontal displacement of the isolation system of 0.88 m to 0.91 m at the MCE; this is within the displacement capacity of the bearings. At the MCE the maximum compression force in an individual outer bearing is 25.3 MN (building BI5a) which is within the capacity of commercially available tension-resistant pendulum bearings. While for individual ground motions, scaled at the MCE, tension force is computed in the outer bearings, in terms of mean response at the MCE, these

bearings approach but do not experience tension; this is why in Table 3 the minimum compression force is reported (1.9 MN for BI5a). Note that if the vertical component of the seismic excitation had been considered, significant tension forces would have possibly been computed in the bearings. Thus if preventing uplift of the isolation system is an objective, tension-resistant bearings are required.

The total force developed in the four NLVDs, $F_{ND,tot}$, buildings BI5a and BI6a is $0.012W_t$ to $0.015W_t$ at DE and $0.014W_t$ to $0.018W_t$ at the MCE. For $F_{ND,tot} = 0.018W_t$ (building BI6a) the corresponding force in each of the NLVDs is $F_{ND} = 0.93$ MN.

At the DE buildings BI5a and BI6a develop shear forces in the wall at the ground level that are $0.12W_s$, and $0.10W_s$, respectively, values that are less than 0.4 times that of the FB building. The corresponding shear forces at the MCE are $0.18W_s$ and $0.14W_s$, respectively (as opposed to $0.33W_s$ for the FB). Compared to the FB building, the same level of shear force reduction is observed along the entire height of buildings BI5a and BI6a. Note that buildings BI5a and BI6a achieve significant reduction of shear forces although they develop larger bending moments at the ground level than the FB building. This is because of the significant reduction of higher-mode response.

For the same reason, these buildings develop average floor accelerations along the height at the DE (0.20 g) and at the MCE (0.24 g to 0.25 g) that are less than 0.33 times the values computed for the FB building. Note the almost constant acceleration in the bottom 75% of the height of the BI buildings (see Figure 4).

We discuss next the response of buildings BI4, BI5b, and BI6b that are designed with isolation system 1 and a wall of M_b equal to 1.1 times the minimum required according to ASCE 7-10. At the DE building BI4 develops an interstory drift ratio of 0.58% and wall tensile strain of 0.69%. The superstructure of buildings BI5b and BI6b responds elastically to the DE with 0.19% to 0.28% interstory drift ratio and 0.12% to 0.23% wall tensile strain. The level of inelastic deformation of the superstructure of these three buildings at the MCE varies significantly, increasing with decrease of T_{is}.

The interstory drift ratio at the MCE of buildings BI6b, BI5b, and BI4 is 0.51%, 0.94%, and 2.02% (0.95 times that of the FB building), respectively. The corresponding values of wall tensile strain are 0.57%, 1.36%, and 2.64%. Note that building BI6b experiences practically elastic response at the MCE (0.57% wall tensile strain and interstory drift ratio of 0.51%). On the other hand building BI4 at the MCE experiences a similar level of inelastic deformations to that of the FB building. Building BI5b develops displacements and forces in the isolation system, shear forces in the wall, and floor accelerations similar to these of building BI5a. Building BI6b develops displacements and forces in the isolation system, shear forces in the wall, and floor accelerations similar to these of building BI6a.

Finally the response of building BI6c, which is the only building that uses isolation system 2, is presented. The superstructure of building BI6c experiences practically elastic response at the MCE, where the wall tensile strain is 0.27% and the interstory drift ratio 0.4%. This building develops the largest horizontal displacement of the isolation system; equal to 0.95 m at the MCE. Building BI6c develops total force in the 4 NFVDs equal to $0.03W_t$ and $0.035W_t$, at the DE and at the MCE, respectively, that is about two times that of building BI6a. This building develops the smallest floor accelerations among all six BI buildings (0.15 g at the DE and 0.21 g at the MCE) with the smoothest shape along the height of the building among all the BI buildings. This is due to the less abrupt change in the horizontal stiffness in isolation system 2 compared to isolation system 1.

Table 3. Modal properties and mean response quantities computed using nonlinear response history analysis (NRHA).

	Building name	**FB**		**BI4**		**BI5a**		**BI5b**		**BI6a**		**BI6b**		**BI6c**	
Modal properties	First mode period, T_1 (s)	2.0		4.3		5.2		5.2		6.2		6.2		6.2	
	First mode mass m_1 divided by m_t	0.66		0.99		0.99		0.99		0.99		0.99		0.99	
	First mode bending moment at ground level, $M_{1,b}$, divided by $V_{1,iso}$*	N/A		$0.39H_t$		$0.37H_t$		$0.38H_t$		$0.37H_t$		$0.37H_t$		$0.37H_t$	
	Excitation level	DE	MCE	DE	MCE	DE	MCE	DE	MCE	DE	MCE	DE	MCE	DE	MCE
Superstructure above ground	Roof drift ratio, D_r / H_s, (%)	1.22	1.75	1.08	2.45	0.81	1.53	0.91	1.93	0.82	1.60	0.84	1.70	0.88	1.71
	Interstory drift ratio, Θ_i, (%)	1.45	2.13	0.58	2.02	0.12	0.30	0.28	0.94	0.15	0.32	0.19	0.51	0.14	0.40
	Average floor acceleration, A_{ave} (g)	0.63	0.83	0.23	0.31	0.20	0.25	0.21	0.25	0.20	0.24	0.20	0.24	0.15	0.21
	Wall shear force, ground level, V_b / W_s	0.30	0.33	0.14	0.23	0.12	0.18	0.11	0.17	0.10	0.14	0.10	0.13	0.11	0.15
	Web shear stress of wall, τ_w / $f'_{c,e}$	0.068	0.075	0.031	0.052	0.021	0.031	0.025	0.039	0.020	0.028	0.023	0.029	0.021	0.029
	Wall long. reinf. tensile strain (%)	2.10	2.75	0.69	2.64	0.05	0.22	0.23	1.36	0.06	0.18	0.12	0.57	0.06	0.27
	Column long. reinf. tensile strain (%)	0.16	0.22	0.06	0.24	0.02	0.03	0.03	0.11	0.02	0.03	0.03	0.05	0.02	0.03
	Slab long. reinf. tensile strain (%)	0.24	0.37	0.08	0.35	0.01	0.04	0.03	0.14	0.01	0.03	0.01	0.07	0.01	0.05
Isolation system	Horizontal displacement, D_{is}, (m)	N/A		0.47	0.70	0.49	0.88	0.48	0.83	0.49	0.91	0.49	0.89	0.53	0.95
	Maximum compressive force of a pendulum bearing ** (MN)			20.9	24.0	21.3	25.3	19.7	22.2	20.0	22.4	19.1	21.0	13.3	15.5
	Minimum compression force of a pendulum bearing ** (MN)			4.1	1.6	4.7	1.9	5.2	2.8	5.8	3.5	5.8	4.0	5.8	3.0
	Total force of the 4 NFVDs, $F_{ND,tot}$ / W_t			N/A		0.012	0.014	0.012	0.014	0.015	0.018	0.015	0.018	0.030	0.035
	Total horizontal force, $F_{is,tot}$ / W_t			0.15	0.21	0.11	0.18	0.11	0.17	0.09	0.14	0.09	0.14	0.10	0.15

* $V_{1,iso}$: first mode shear force at the level of the isolation system,** for isolation system 2 this is the force of an individual linear bearing.

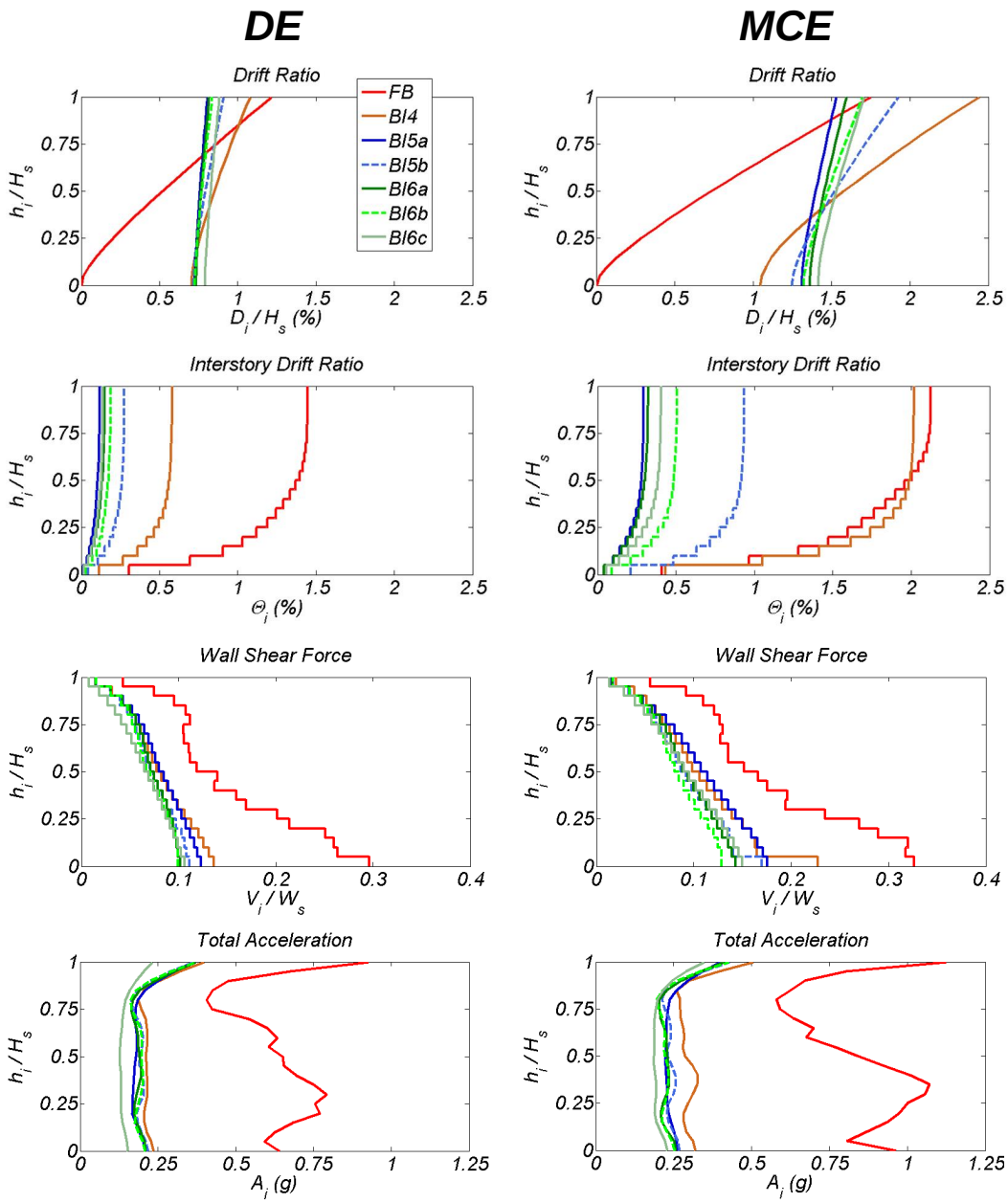

Figure 4. Mean responses along the building height at the DE and MCE hazard level.

5.3 Response History Analysis to Unscaled Near-Fault Pulse-Type Ground Motions

The response of buildings FB, BI5a, BI6a, BI6b, and BI6c to four unscaled historical pulse-type near-fault ground motions is considered next.

Depending on the site location with respect to the fault rupture, near-fault ground motions can include strong acceleration, velocity, and displacement pulses, as a result of directivity effects, with predominant period, T_p, that increases with increasing earthquake magnitude [38, 39]. Motions that include strong long-period pulses can

impose large demands in long-period FB and BI tall buildings that may exceed these expected at the MCE.

Table 4 summarizes the earthquakes of magnitude larger than M7 for which, ground motion records at a distance from the fault rupture, R_{rup}, less than 10 km exist. The number of records with R_{rup} < 10 km for each of these earthquakes is also listed in this Table. All ground motions included in the PEER database [40] are considered in the creation of Table 4. Note that not all of the 47 motions included in Table 4 were affected by forward directivity. More than two-thirds of these 47 records were recorded during the 1999 M7.6 Chi-Chi, Taiwan, earthquake and only 5 in U.S. The small number of near-fault records from large magnitude (M > 7.0) earthquakes results in large uncertainty in determining the seismic hazard close to fault rupture and makes problematic the selection of pulse-type near-fault motions with specific combination of key characteristics such as earthquake magnitude, source mechanism, R_{rup}, and site class.

Table 4. Near-fault records with R_{rup}<10 km from earthquakes of magnitude $M \geq 7.0$.

	Cape Mend. U.S.	Duzce Turkey	Landers U.S.	Tabas Iran	Kocaeli Turkey	Chi-Chi Taiwan	Wechuan China	Denali Alaska
Year	1992	1999	1992	1978	1999	1999	2008	2002
Magnitude	7.0	7.1	7.4	7.4	7.5	7.6	7.9	7.9
Number of records	2	6	1	1	2	32	2*	1

Notes: *PEER database does not include the motions from the 2008 M7.9 Wenchuan, China earthquake.

The main characteristics of the four pulse-type near-fault ground motions used in the analysis of the FB and the four BI buildings are listed in Table 5. The ground velocity time seriess and the linear SDOF spectra of the four motions are shown in Figures 5 and 6, respectively. The fault-normal horizontal component is considered for all four motions. The characteristics summarized in Table 5 are the peak ground velocity (PGV), the average shear wave velocity in the top 30 m, $\overline{v_s}$, and the predominant period, T_p, of the pulse contained in the ground velocity time history. The T_p as computed using wavelet analysis [38] is reported here. For all these four motions R_{rup} < 2.1 km. The linear spectral displacements, *Sd*, of the four motions exceed the MCE design spectrum over different period ranges for the site considered herein, with R_{rup} = 2 km from the Hayward fault, which has the potential to produce an M7.2 earthquake [41]. For T = 5 s motions TCU 52, 68 and Tabas result in *Sd* equal to about 1.5 times that of the MCE design spectrum. For T = 6 s motions TCU 52, 68 result in *Sd* equal to about 1.45 times that of the MCE design spectrum.

These four motions are selected because they include very strong long-period pulses that result in large demands, exceeding these at the MCE, in the response of the buildings studied here. Note that one or more of their key characteristics (see Table 5) are not consistent with the site studied for the following reasons: (1) the number of historically recorded near-fault motions affected by forward directivity with all their key characteristics consistent with the site studied here is practically zero; and (2) because this investigation aims to study how the FB and the selected BI buildings would respond in some of the most severe near-fault motions ever recorded.

Table 5. Characteristics of the four near-fault ground motions.

Station	Earthquake name, year and magnitude	Source mechanism	$\overline{v_s}$ (m/sec)	PGV (m/s)	T_p (sec)
El Centro Array #6 (ElCen6)	Imperial Valley, 1979, M6.5	Strike slip	206	1.12	3.9
Tabas	Tabas, Iran, 1978, M7.4	Reverse	767	1.21	5.3
TCU52	Chi-Chi, Taiwan, 1999, M7.6	Reverse	579	1.65	12.7
TCU68			487	1.85	12.2

Note: For all four motions R_{rup} < 2.1 km

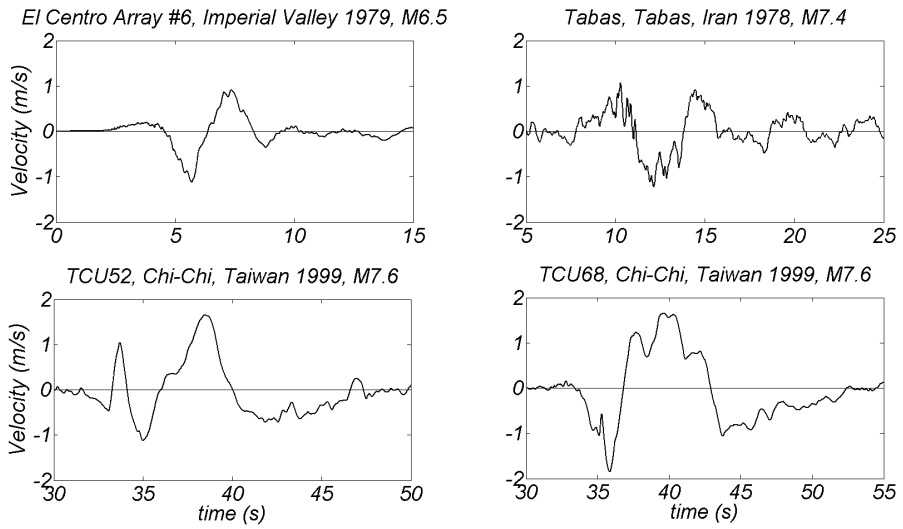

Figure 5. Ground velocity time history of the four near-fault ground motions.

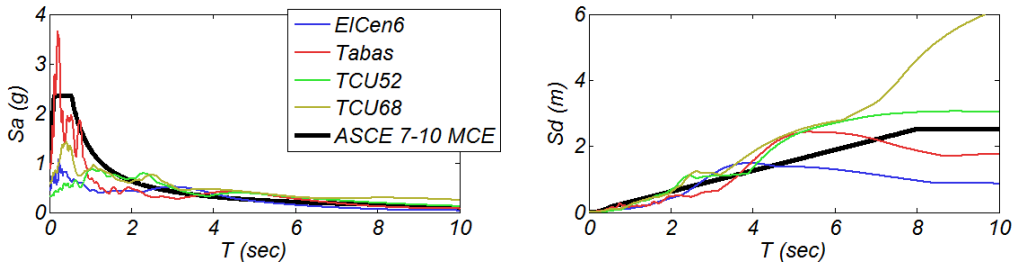

Figure 6. Acceleration and displacement spectra for linear response, ζ=5%, of the four near-fault historical records compared to the design spectra for the Berkeley, California, site.

Among all the motions currently available in the PEER database, TCU68 results in the largest *Sd* in the period range of 6 to 10 s, TCU52 and Tabas result in the third largest *Sd* at T = 5 s (after TCU68 and TCU65 recorded in Chi-Chi earthquake), and ElCen6 results in in the fourth largest (after TCU 52, 65, and 68) *Sd* at T= 3 s, all for ζ=5%. Note also that motions TCU52 and TCU68 also include some distinct pulses of period about 2.5 s in addition to the 12.7 s, and 12.2 s periods described above, resulting in local peaks in *Sd* for T = 2.5 s. Motions TCU 52 and 68 result in the largest *Sd* for T = 2.2 to 2.5 s (T_1 = 2 s for the FB building) among all motions included in the PEER database.

Figure 7 shows the NRHA results of the five buildings studied when subjected to the four unscaled near-fault motions. The FB building reaches roof drift ratios ranging between 1.6% and 3.7% (1.75% at the MCE), interstory drift ratios ranging between 1.8% and 4.0% (2.13% at the MCE), shear force in the wall ranging between 0.23W_s and 0.37W_s (0.33W_s at the MCE), floor accelerations (average along the height of the building) ranging between 0.4 g and 1.0 g (0.83 g at the MCE), and wall tensile strain ranging between 2.9% and 5.2% (2.75% at the MCE).

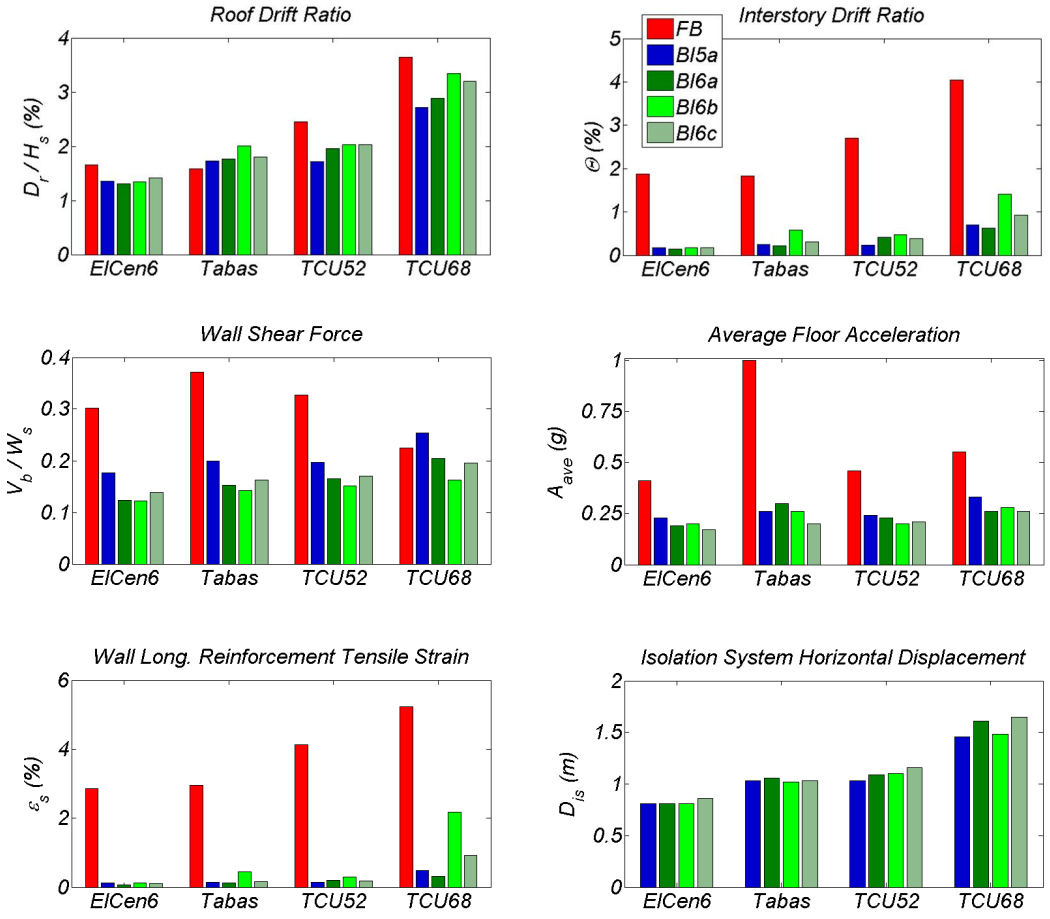

Figure 7. Response of the FB building and the four BI buildings to the four historical near-fault ground motions.

The four BI buildings attain less than 1% interstory drift in all four motions, except building BI6b for motion TCU68 where the interstory drift is 1.4%. A comparison among the four BI buildings demonstrates that building BI6b experiences the largest interstory drift for all four motions. The four BI buildings experience less than 0.66 times the shear force of the FB building for all motions except TCU68. Building BI5a results in the largest shear force in the wall among the four BI buildings. All four BI buildings experience less than 0.55 times the average (along the height of the building) floor acceleration the FB building developed.

The horizontal displacement of the isolation system of the four BI buildings ranges between 0.8 m and 0.86 m for motion ElCen6 which is 0.85 times, on average, the corresponding displacement at the MCE. For the Tabas motion, D_{is} is between 1.02 m to 1.06 m that is about 1.1 times that at the MCE. The corresponding range of D_{is} for motion TCU52 is between 1.03 to 1.16 m (building BI6c). Motion TCU68 results in the largest D_{is} = 1.46 m to 1.65 m for all four BI buildings. The level of D_{is} reached for TCU68 exceeds the displacement capacity of commercially available LPRBs and approaches or exceeds that of tension-resistant pendulum bearings.

6. SUMMARY AND CONCLUSIONS

This study investigated the seismic response of six base-isolated (BI) buildings with 20 stories above ground and compared it to that of a similar fixed-base (FB) building. All buildings were hypothetically located in downtown Berkeley, California, 2 km from the Hayward fault, and were designed with a core wall to provide most of the lateral force resistance above ground. All buildings were designed according to ASCE 7-10 except that a single horizontal component of seismic excitation was used in the 2-D nonlinear response history analysis (NRHA). The design base shear force of the FB building was $0.098W_s$ (W_s: the seismic weight of the building above ground). Buildings BI4, BI5a, BI5b, BI6a, and BI6b used isolation system 1 that combined 16 tension-resistant pendulum bearings and 8 nonlinear fluid viscous dampers (NFVDs). Building BI6c used isolation system 2 that combined 12 very low-friction (μ=0.3%) tension-resistant linear bearings, 12 lead-plug rubber bearings (LPRBs) and 8 NFVDs. Isolation periods T_{is} equal to 4 s (building BI4a), 5 s (buildings BI5a, and BI5b), and 6 s (buildings BI6a, and BI6b) were studied. Building BI5a used a wall with flexural strength 2.2 times the minimum required by ASCE 7-10. Buildings BI6a, and BI6c used a wall with M_b equal to 1.8 times the minimum required while for buildings BI4a, BI5b, BI6b M_b was equal to 1.1 times the minimum required. Numerical models of all seven buildings were subjected (uni-axial excitation) to a set of 14 ground motions scaled to match approximately the DE and the MCE design spectra. All buildings except BI4 and BI5b were also subjected to four unscaled historical near-fault ground motions, which includ strong long-period pulses. The linear single degree of freedom displacement spectra values for these motions were up to 1.5 times these of the MCE-level design spectrum for periods 5 s to 6 s. Based on the results of the analysis the following conclusions are drawn:

1) The FB building developed significant inelastic deformations both at the DE and MCE level of shaking. The mean roof drift ratio at the DE and MCE levels was 1.22% and 1.75%, respectively, while the corresponding peak interstory drift ratio along the height of the building was 1.45% and 2.13%, respectively. The damage potential of the core wall of the FB building increased in response to the concurrent large shear stresses

and inelastic deformations. The shear force in the core wall at the ground level at the DE and MCE level was $0.30W_s$ and $0.33W_s$, respectively. The level of shear stresses in the web of the wall at the DE and MCE was $0.068\,f'_{c,e}$ and $0.075\,f'_{c,e}$ respectively, where $f'_{c,e}$ = 72 MPa was the expected compressive strength of concrete. The maximum allowed stress by ACI 318-11 was $0.0078\,f'_{c,e}$. Tests of non-planar walls with longitudinal steel ratios and axial load ratios 0.8 to 1.2 times and 0.8 to 1.6 times, respectively, that of the wall considered herein experienced significant damage, including bar buckling, and crushing of concrete at drift ratios of 1.5% to 2.5%.

2) The FB building resulted in floor accelerations (average along the building height) equal to 0.63g (1.2 PGA) and 0.83g (1.1 PGA) at the DE and at the MCE, respectively.

3) Compared to the response of the FB building, commercially available isolation devices used in the design of the BI buildings resulted in an isolated superstructure for buildings BI5a, BI6a, BI6b, and BI6c that remained practically elastic at the MCE, while reduced significantly interstory drifts, shear forces, and floors accelerations. Buildings BI5a, BI6a, BI6b, and BI6c developed less than 0.95 m of horizontal displacement of the isolation system. The outer bearings of these buildings approached but did not reach the point of experiencing tension (in terms of average response to the 14 ground motions scaled at the MCE). If the vertical component of excitation is considered, significant tension forces should be expected. These buildings developed less than 0.51% interstory drift at the MCE and less than 0.57% tensile strain in the wall, while floor accelerations (average along the building height) were less than 0.25 g at the MCE, (0.83 g for the FB building). The shear force in the wall at the ground level at the MCE of these buildings was $0.13W_s$ to $0.18W_s$ ($0.33W_s$ for the FB building).

4) The level of inelastic deformations of the core wall that buildings BI6b, BI5b, BI4 (all three had a wall with flexural strength, M_b, 1.1 times the minimum required by ASCE 7-10) developed at the MCE increased with decrease of T_{is}. Interstory drifts increased from 0.51% (building BI6b) to 0.94% in building BI5b and to 2.02% (2.13% for the FB building) in building BI4.

5) In response to the four unscaled near-fault ground motions, the FB building developed significant inelastic deformations with interstory drift ratio that ranged from 1.8% to 4%. The corresponding range of tensile strain of the longitudinal reinforcement in the wall was 2.9% to 5.2%. All four BI buildings developed less than 1% interstory drift ratio except building BI6b subjected to motion TCU68. The horizontal displacements of the isolation systems were 0.81 m to 1.16 m for motions ElCen6, Tabas, and TCU52. For the TCU68 motion, the D_{is} of the four BI buildings ranged from 1.45 m (BI5a) to 1.65 m (BI6c). Commercially available tension-resistant pendulum bearings and NFVDs with displacement capacity up to 1.5 m achieved a practically elastic response of the superstructure, even for this extremely rare and high-intensity motion.

REFERENCES

1. Klemencic R, Fry A, Hooper JD, Morgen BG. Performance-based design of ductile concrete core wall buildings – issues to consider before detailed analysis. *Structural Design of Tall and Special Buildings* 2007; **16**:599–614.

2. Aguilar J, et al. The Mexico earthquake of September 19, 1985 – statistics of damage and of retrofitting techniques in reinforced concrete buildings affected by the 1985 earthquake. *Earthquake Spectra* 1989; **5**(1):145-151.
3. Westenenk B, et al. Response of reinforced concrete buildings in Concepcion during the Maule earthquake. *Earthquake Spectra* 2012; **28**(S1):S257-S280.
4. Elwood, K. J., Pampanin, S., and Kam, W.Y., 2012. NZ 22 February 2011 Christchurch Earthquake and Implications for the Design of Concrete Structures, in *Proceedings, International Symposium on Engineering Lessons Learned from the 2011 Great East Japan Earthquake*, Tokyo, Japan, pp.1157-1158.
5. Tsai KC, Hsiao CP, Bruneau M. Overview of building damages in 921 Chi-Chi earthquake. *Earth. Engineering and Engineering Seismology* 2000; **2**(1):93–108.
6. Seed HB, Romo MP, Sun JI, Jaime A, Lysmer J. The Mexico earthquake of September 19, 1985 – relationships between soil conditions and earthquake ground motions. *Earthquake Spectra* 1988; **4**(4):687-729.
7. Boroschek RL, Contreras V, Kwak DY, Stewart JP. Strong ground motion attributes of the 2010 Mw 8.8 Maule, Chile, earthquake. *Earthquake Spectra* 2012; **28**(S1):S19-S38.
8. Moehle J, Bozorgnia Y, et al. Case studies of the seismic performance of tall buildings designed by alternative means. Task 12 report for the Tall Buildings Initiative. *PEER Report 2011/05*, University of California, Berkeley, CA, 2011.
9. Panagiotou M, Restrepo JI. Dual-plastic hinge design concept for reducing higher-mode effects on high-rise cantilever wall buildings. *Earthquake Engineering and Structural Dynamics* 2009; **38**(12):1359–1380.
10. Calugaru V, Panagiotou M. Response of tall cantilever wall buildings to strong pulse-type seismic excitation. *Earthquake Engineering and Structural Dynamics* 2012; 41(9):1301-1318.
11. American Society of Civil Engineers. *Minimum Design Loads for Buildings and Other Structures.* ASCE 7-10, Reston, VA, 2010.
12. American Concrete Institute. *Building Code Requirements for Structural Concrete (ACI 318-11) and Commentary*. ACI 318-11, ACI Committee 318, Farmington Hills, 2011.
13. Structural Engineers Association of Northern California. Seismic design and review of tall buildings using non-prescriptive procedures. *Recommended Administrative Bulletin, San Francisco*, 2007.
14. Willford M, Whittaker A, Klemencic R. Recommendations for the seismic design of high-rise buildings. *Council on Tall Buildings and the Urban Habitat, Draft for Comment*, February 21, 2008; 28.
15. Los Angeles Tall Buildings Structural Design Council. *An Alternative Procedure for Seismic Analysis and Design of Tall Buildings Located in the Los Angeles Region*, 2011.
16. Tall Buildings Initiative, Guidelines for Performance-Based Seismic Design of Tall Buildings, *Pacific Earthquake Engineering Research Center*, Report No. 2010/05.
17. Priestley MJN, Calvi GM, Kowalsky, MJ, *Displacement-Based Seismic Design of Structures*, 2007, Pavia, Italy.
18. Dynamic Isolation Systems (DIS). http://www.dis-inc.com/index.html [accessed November 2012].
19. Earthquake Protection Systems. http://www.earthquakeprotection.com/ [accessed November 2012].
20. THK. http://www.thk.com/?q=eng/node/260 [accessed November 2012]

21. Taylor Devices Inc. http://www.taylordevices.com/dampers-seismic-protection.html [accessed September 2012].
22. Fujita T. Seismic isolation rubber bearings for nuclear facilities. *Nuclear Engineering Design* 1991; **127**:379-391.
23. Komuro T, et al. Development and realization of base isolation system for high-rise buildings. *Journal of Advanced Concrete Technology* 2005; **3**(2):233–239.
24. Ryan KL, et al. Aspects of isolation device behavior observed from full-scale testing of an isolated building at E-Defense. *Proceedings of the 20th Analysis & Computation Specialty Conference* 2012; p. 25-36.
25. Pan P, et al. Base-isolation design practice in Japan: introduction to the post-Kobe approach. *Journal of Earthquake Engineering* 2005*;* **9**(1):147–171.
26. Kani N. Current state of seismic-isolation design. *Journal of Disaster Research* 2009*;* **4**(3):175–181.
27. Sayani PJ, Ryan KL, Comparative evaluation of base-isolated and fixed-base buildings using a comprehensive response index, ASCE *Journal of Structural Engineering* 2009; **135**(6): 2952-2968.
28. Hall JF, Ryan KL, Isolated buildings and the 1997 UBC Near-Source Factors, *Earthquake Spectra*, 2000, 16(2): 393-411.
29. Morgan TA, Mahin SA. The use of base isolation systems to achieve complex seismic performance objectives. *PEER*, PEER Report 2011/06.
30. Kikuchi M, Black CJ, Aiken ID. On the response of yielding seismically isolated structures. *Earthquake Engineering and Structural Dynamics* 2008; **37**(5):659-679.
31. Walters M. The seismic retrofit of the Oakland City Hall. *SMIP03 Seminar Proceedings*; p. 149-163.
32. Kelly JM, Konstantinidis DA. Mechanics of rubber bearings for seismic and vibration isolation, 2011, United Kingdom
33. Open System for Earthquake Engineering Simulation (OpenSees). opensees.berkeley.edu [accessed November 2012].
34. Sittipunt C, Wood S, Finite element analysis of reinforced concrete walls, report to the National Science Foundation, University of Illinois at Urbana-Champaign, 1993.
35. Thomsen JH, Wallace JW. Displacement-based design of slender reinforced concrete structural walls - experimental verification. *Journal of Structural Engineering*, 2004; 130(4): 618-630.
36. Beyer K, Dazio A, Priestley MJN. Quasi-static cyclic tests of two U-shaped Reinforced Concrete Walls. *Journal of Earth. Eng.* 2008, 12(7): 1023-1053.
37. Restrepo JI, Lang AF. Study of loading protocols in light-garage stud partition walls. *Earthquake Spectra* 2011; **27**(4):1169-1185.
38. Mavroeidis GP, Papageorgiou AS. A Mathematical Representation of Near-Fault Ground Motions, *Bull. Seism. Soc. Am.*, 2003, 93: 1099-1131.
39. Baker JW, Quantitative classification of near-fault ground motions using wavelet analysis. *Bulletin of the Seismological Society of America*, 2007, 97 (5): 1486-1501.
40. Pacific Earthquake Engineering Research Center, Strong Motion Database, http://peer.berkeley.edu/peer_ground_motion_database, (accessed 09/23/2012).
41. Aagard B, et al. Ground-motion modeling of Hayward fault scenario earthquakes, Part I: Construction of the suite of scenarios, Bull. of the Seism. Soc. of Amer., 100(6), 2010, pp:2927-2944.